APPLICATIONS OF
MODELLING AND SIMULATION
http://arqiipubl.com/ams eISSN 2600-8084 VOL 9, 2025, 264-272

PID Control and Input Shaping for Quadrotor UAV Stabilization and Payload Swing Reduction

Liyana Ramli*, Izzuddin M. Lazim, Amalin Aisya Awi and Aina Syazwin Shukor

Faculty of Engineering and Built Environment, Universiti Sains Islam Malaysia, 71800 Nilai, Negeri Sembilan, Malaysia

*Corresponding author: lyanaramli@usim.edu.my

Submitted 28 March 2025; Revised 20 June 2025; Accepted 25 June 2025; Available online 29 June 2025.

Abstract: Controlling an under-actuated quadrotor system with a suspended payload poses significant challenges due to payload–attitude coupling, where excessive payload swing can adversely affect the quadrotor's stability and performance. This study proposes an optimal Unity Magnitude Zero Vibration (UMZV) input shaper to minimize payload swing, combined with a feedback control strategy for managing the quadrotor's position and attitude. To enhance swing suppression, the input shaper parameters are optimized using the Particle Swarm Optimization (PSO) algorithm. In addition, a PID controller is employed to regulate the quadrotor's motion, ensuring effective swing suppression while maintaining desirable attitude and position control. Simulation results demonstrate that the proposed control scheme achieves a substantial reduction in payload swing of at least 65.28% compared to existing methods. Furthermore, it delivers improved attitude and position tracking performance, confirming its effectiveness in managing the coupled dynamics of the quadrotor–payload system.

Keywords: Quadrotor; PSO; Payload swing; Position control; UMZV shaper.

1. INTRODUCTION

Quadrotors carrying suspended payloads represent a class of unmanned aerial vehicles (UAVs) that offer practical solutions for rapid delivery to inaccessible or remote locations. UAVs have proven particularly valuable in the medical field, where they are used to transport blood and medications efficiently, especially in rural areas [1]. Besides that, the quadrotor can be very useful during natural disasters such as floods, as it can supply medicines and food to the trapped victims. Compared to a quadrotor without a payload, designing control systems for one carrying a suspended load is more challenging [2], [3]. Payload swing during flight can significantly destabilize the quadrotor, compromising safety and performance. Despite these challenges, quadrotors continue to attract considerable attention in both research and industry, particularly for aerial cargo delivery, due to their advantages such as precise hovering, high maneuverability, and vertical takeoff and landing capabilities. However, the conventional technique to transport the payload by air using a gripper that is equipped on the quadrotor may result in a slow attitude response due to additional inertia [4]. An alternative and often more efficient method is to suspend the payload using a cable. This approach is especially beneficial when transporting hazardous materials or objects with distributed mass. However, it introduces the additional complexity of controlling payload-induced vibrations and swing. Therefore, this research focuses on the control of a quadrotor with a suspended load, addressing a practically significant problem to ensure safe and stable payload transportation.

Flying with a hanging cargo can be challenging because there are only four independent control inputs and eight degrees of freedom [5]. In [6], the quadrotor position and attitude were controlled by a model-based control system. However, the payload swing was significantly induced due to the quadrotor motion. Hence, input shaping was combined to regulate the swing efficiently. In another research, a hierarchical control system based on energy coupling was suggested for both payload swing reduction and quadrotor positioning [7]. In [8], as parameter uncertainty may affect the overall control performances, an adaptive approach was employed for anti-swing control and the approach was designed to compensate for the swing response due to the unknown cable length. Aerial control of several UAVs carrying heavy loads was also put into place in case of disturbance [9].

Numerous studies have implemented input shaping techniques in quadrotor systems to enhance payload swing suppression efficiency [10], [11], [12]. For instance, input-shaping-based velocity control has been shown to be effective in mitigating payload oscillations in quadrotors [13]. In a helicopter system, a combined input shaping with a feedback controller was proposed [14] where a hybrid control was utilized to eliminate the payload swing of the system. This method integrated input shaping with model-following control to suppress slow, large-amplitude oscillations, while the feedback controller maintains system stability. Similarly, in a double-pendulum bridge crane system, a feedback controller was employed to regulate the trolley position, while input shaping was applied to reduce deflections during initial acceleration [15], while input shaping was

utilized to lessen the initial acceleration deflection. Input shaping has also been experimentally validated for disturbance rejection under varying system stiffness conditions [16]. In another study, an enhanced input shaper called the symmetric perturbation based extra insensitive input shaper was proposed for crane systems to improve swing suppression, particularly in the low frequency region [17]. However, this method increased the total motion time due to a longer shaping duration. Additionally, a reversion input shaping technique was proposed for flexible systems [7] , which redistributed the excitation frequency of the reference trajectory based on shaping principles. Although effective, this method slightly compromised robustness.

For the input shaping design to achieve an effective swing reduction, precise system parameters are necessary. Furthermore, because a traditional shaper is developed based on a linear plant, its efficiency tends to decrease for non-linear systems. An approach that can optimize the shaper parameters based on a nonlinear system is preferred for an accurate shaper design. Thus, this research proposes a particle swarm optimization-based unity magnitude zero vibration shaper (PSOUMZV) for an efficient payload swing reduction in order to manage the effect of the system's nonlinearities. With no prior knowledge of the system characteristics, the PSO may optimize the UMZV shaper efficiently. Furthermore, the UMZV shaper, which was developed using a linear model, is utilized as a comparison to support the efficacy of the proposed approach. The proportional derivative (PD) controller is utilized to control the position and attitude of the quadrotor system. MATLAB simulations are used in this work to assess the controller's performance. The main strength of this paper can be concluded as follows:

- The PSO can be used to immediately obtain the ideal shaper parameters, eliminating the need for the natural frequency and damping ratio in the shaper design.
- It was the linearized model that served as the basis for the majority of input shaping approaches. A nonlinear model will be used to determine the ideal shaper parameters using the proposed approach.

2. MODEL DESCRIPTIONS

2.1 Quadrotor Dynamics

This section presents the quadrotor dynamics consisting of four inputs, namely thrust T, pitch torque τ_ϕ, roll torque τ_θ and yaw torque τ_ψ. These inputs can be written as,

$$\begin{bmatrix} T \\ \tau_\phi \\ \tau_\theta \\ \tau_\psi \end{bmatrix} = \begin{bmatrix} k_1 & k_2 & k_3 & k_4 \\ lk_1 & 0 & -lk_3 & 0 \\ 0 & lk_2 & 0 & -lk_4 \\ b_1 & -b_2 & b_3 & -b_4 \end{bmatrix} \begin{bmatrix} {\omega_1}^2 \\ {\omega_2}^2 \\ {\omega_3}^2 \\ {\omega_4}^2 \end{bmatrix} \tag{1}$$

The angular speed, thrust coefficient, and torque coefficient of each motor are denoted by the symbols, ω_i, k_i and b_i. The horizontal distance between the motor's center and the center of gravity is indicated by the symbol, l. From quadrotor local space to inertial globe space, the rotation matrix R can be expressed as

$$R(\boldsymbol{\xi}) = \begin{bmatrix} \cos\theta\cos\psi - \sin\phi\sin\theta\sin\psi & -\cos\phi\sin\psi & \cos\psi\sin\theta + \cos\theta\sin\phi\sin\psi \\ \cos\theta\sin\psi + \sin\phi\sin\theta\cos\psi & \cos\phi\cos\psi & \sin\psi\sin\theta - \cos\psi\cos\theta\sin\phi \\ -\cos\phi\sin\theta & \sin\phi & \cos\phi\cos\theta \end{bmatrix} \tag{2}$$

$r = [x,\ y,\ z]^{\mathrm{T}}$ denotes the quadrotor position, $\boldsymbol{\xi} = [\phi,\ \theta,\ \psi]^{\mathrm{T}}$ denotes the attitude of the quadrotor, namely pitch ϕ, roll θ and yaw ψ. The equation of motion is given as,

$$\ddot{r} = \frac{1}{m_q}(F_g + F_d + RT_r + RF_p) \tag{3}$$

where m_q, F_g and F_d represent the mass, gravitational force, and drag force of the quadrotor, respectively, whereas F_p is the force of payload on the quadrotor. T_r is the trust vector in the quadrotor local coordinate given as $[0,\ 0,\ T]^{\mathrm{T}}$. The gravitational force and drag forces can be formulated as,

$$F_g = \begin{bmatrix} 0 \\ 0 \\ -m_q g \end{bmatrix} \tag{4}$$

$$F_d = -\frac{1}{2} C_d A \rho_{air} \|\dot{r}\| \dot{r} \tag{5}$$

where C_d, A and ρ_{air} are the drag coefficient, drag area and air density respectively. In rotational dynamics, the equation of motion can be written as,

$$\ddot{\xi} = I^{-1}\left(\tau_d + \tau + \tau_p - \dot{\xi} \times \left(I\dot{\xi}\right)\right) \tag{6}$$

The diagonal inertia matrix, torque owing to drag, and torque due to the payload are represented by the symbols I, τ_d and τ_p, respectively. τ_d can be expressed as

$$\tau_d = (Rr_{cop}) \times F_d \tag{7}$$

where the center of pressure is r_{cop}. When applied above the quadrotor's center of gravity, the drag torque would act as damping and oppose the motion in this simulation. As a result, the equilibrium angle is smaller than expected and the system becomes less maneuverable but more stable [18]. The vector distance between the quadrotor's center of gravity and the payload attachment point, taking payload dynamics into account, is as follows:

$$r_{offset} = [0 \quad 0 \quad -d] \tag{8}$$

where d is the distance measured in z-axis. The payload position r_l measured from the offset point is,

$$r_l = -L_p \begin{bmatrix} -\cos\phi_p \sin\theta_p \\ \sin\phi_p \\ \cos\theta_p \cos\phi_p \end{bmatrix} \tag{9}$$

where L_p, ϕ_p and θ_p are the cable length, tangential and orthogonal payload angles respectively. The payload position r_p that is measured from the quadrotor body is,

$$r_p = r_l + r_{offset} \tag{10}$$

The payload velocity can be calculated as,

$$\dot{r}_p = \dot{r} + \dot{r}_l + \dot{\xi} \times r_l \tag{11}$$

and the payload acceleration is,

$$\ddot{r}_p = \ddot{r} + \ddot{r}_l + \ddot{\xi} \times r_l + 2\dot{\xi} \times \dot{r}_l + \dot{\xi} \times \left(\dot{\xi} \times r_l\right) \tag{12}$$

The relative gravity of the payload is,

$$g_\xi = g \begin{bmatrix} -\cos\phi \sin\theta \\ \sin\phi \\ \cos\theta \cos\phi \end{bmatrix} \tag{13}$$

The drag acceleration is given as,

$$f_\xi = R^T \frac{F_{dp}}{m_p} \tag{14}$$

where F_{dp} is the payload drag force given as,

$$F_{dp} = -\frac{1}{2} C_{dp} A_p \rho_{air} \|\dot{r}_p\| \dot{r}_p \tag{15}$$

where C_{dp} and A_p are the payload drag coefficient and payload drag area respectively. The quadrotor's payload force and torque are:

$$F_p = m_p(\ddot{r}_p - g_\xi + f_\xi) \tag{16}$$

Hence, the equations of motion for the payload are,

$$\begin{aligned} \ddot{\theta}_p = &-\cos\theta_p \sin\theta_p \dot{\phi}^2 + 2t \tan\phi_p \dot{\theta}_p \dot{\phi}_p \dot{\psi} + \cos\theta_p \sin\theta_p \dot{\psi}^2 + \dot{\phi}(2\sin\theta_p \dot{\phi}_p + \left(\cos^2\theta_p - \sin^2\theta_p\right)\dot{\psi}) + \\ &\tan\phi_p \dot{\theta}\left(\cos\theta_p \dot{\phi} - 2\dot{\phi}_p + \sin\theta_p \dot{\psi}\right) + (\cos\theta_p(f_x + g\cos\phi\sin\theta) + (f_z - g\cos\theta\cos\phi)\sin\theta_p + \cos\theta_p \ddot{x} + \\ &\cos^2\phi_p \sin\theta_p \ddot{z})/L_p/\cos\phi_p + \ddot{\theta} + \sin\theta_p \tan\phi_p \ddot{\phi} - \cos\theta_p \tan\phi_p \ddot{\psi} \end{aligned} \tag{17}$$

$$\ddot{\phi}_p = -\sin\phi_p \cos\phi_p \dot{\theta}^2 - \sin\phi_p \cos\phi_p \dot{\theta}_p^2 + \sin\phi_p \cos\phi_p \left(\sin\theta_p \dot{\phi} - \cos\phi_p \dot{\psi}\right)^2 +$$

$$2\cos^2\phi_p\,\dot{\theta}_p(-\sin\theta_p+\cos\theta_p\,\dot{\psi})+\dot{\theta}\left(2\sin\phi_p\cos\phi_p\,\dot{\theta}_p+(\cos^2\phi_p-\sin^2\phi_p)(\sin\theta_p\,\dot{\phi}-\cos\theta_p\,\dot{\psi})\right)-(\cos\phi_p\,(f_y-g\sin\phi)+(-f_z\cos\theta_p+g(\sin\theta\sin\theta_p+\cos\theta\cos\theta_p)\cos\phi+f_x\sin\theta_p)\sin\phi_p+\cos\phi_p\,\ddot{y}-\sin\phi_p\,(-\sin\theta_p\,\ddot{x}+\cos\theta_p\,\ddot{z}))/L_p+\cos\theta_p\,\ddot{\phi}+\sin\theta_p\,\ddot{\psi} \quad (18)$$

Table 1 shows the parameters values of the quadrotor system.

Table 1. System parameters.

Parameter	Description	Value	Unit
m_q	Quadrotor mass	1	kg
g	Gravitational force	9.81	ms^{-2}
I_{xx}	Moment of inertia along the x-axis	$6815763.88e^{-9}$	kgm^2
I_{yy}	Moment of inertia along the y-axis	$6801641.50e^{-9}$	kgm^2
I_{xx}	Moment of inertia along the z-axis	$4548279.56e^{-9}$	kgm^2
A	Estimation of cross-sectional area	0.025	m^2
m_p	Payload mass	0.08	kg
L_p	Length of cable	1	m
r_{susp}	Suspension points of the cable	-0.05	m
A_p	Estimation of the cross-sectional area of the payload	$\pi\ (0.0508^2)$	m^2
ρ_{air}	Air density	1.22	kgm^3
C_d	Drag coefficient	1	-
C_{dp}	Drag coefficient payload	0.5	-

3. CONTROLLER DESIGN

This section presents a hybrid strategy utilizing the UMZV shaper with feedback controllers to achieve an accurate quadrotor position and attitude, together with swing suppression of the payload. In addition, the PSO algorithm is utilized to obtain an optimal design of the shaper parameters.

3.1 UMZV-PD Design

Similar to crane systems with finite-state actuation (off, slow, and fast), quadrotors can benefit from discrete command profiles enabled by input shaping. Hence, one of the shapers that can create these commands to imitate the crane system with finite-state actuation is a unity magnitude input shaping (UMZV). Negative impulse amplitudes can be used to create a shorter shaper than ZV shapers with positive impulse amplitudes. This is because impulse amplitudes are limited to either 1 or -1 in order to generate a time-optimal command. This restriction is used to generate the UMZV shaper, which is provided as [19]

$$\begin{bmatrix}A_i\\t_i\end{bmatrix}=\begin{bmatrix}1 & -1 & 1\\0 & t_2 & t_3\end{bmatrix} \quad (19)$$

where

$$t_2=2\pi/\omega_d(1/6+0.272\zeta+0.203\zeta^2)$$
$$t_3=2\pi/\omega_d(1/3+0.005\zeta+0.179\zeta^2) \quad (20)$$

To achieve an accurate design of the UMZV shaper for an efficient payload swing reduction, the shaper is designed based on a non-linear model utilizing the PSO algorithm. Shaper parameters that match the position vector of the, $i\text{-}th$. particle in the search space were used to assign the PSO control variables. A range of [0.1,0.6] was allocated to each control variable. PSO's population was set at forty. At the commencement of the training process, a group of particles was randomly initiated in the swarm, and the total number of particles was set at 40. Each particle is allocated in a D-dimensional space as a point, and its locations updated with velocity in the search space would ultimately achieve optimal solutions. The velocity of the i^{th} particle is given by

$$V_{id}^{t+1}=\omega V_{id}^{t}+c_1r_{1d}^{t}[pb_{id}^{t}-x_{id}^{t}]+c_2r_{2d}^{t}[gb_{d}^{t}-x_{id}^{t}] \quad (21)$$

$$x_{id}^{t+1}=x_{id}^{t}+V_{id}^{t+1} \quad (22)$$

where the current iteration number is denoted by t, i, and $d\in[1,D]$. Acceleration coefficients were chosen at 1.5 for the parameters c_1 and c_2. Between [0, 1], the random integers r_1 and r_2 were assigned. The inertia weight, ω, was set as follows in order to effectively regulate the momentum and the capability in terms of exploring and exploiting the particles toward finding a good ideal solution:

$$\omega^{t+1} = \omega_{max} - (\frac{\omega_{max} - \omega_{min}}{t_{max}})t \tag{23}$$

where ω_{max} and ω_{min} are the maximum and minimum inertia weight values, which were set to 0.9 and 0.4, respectively. t_{max} is the maximum iteration number. To decrease the swing angle, all particles were assessed using their respective objective function, J, which is based on the integral absolute error (IAE).

Figure 1 shows the block diagram of the proposed technique for this simulation. The desired input for the x and y axes for the payload swing is represented by U_x and U_y . Table 2 shows the shaper's parameter for the proposed method.

Table 2. Shaper's parameters for the proposed method.

Shaper parameters	Amplitude			Time locations (s)			
				PSOUMZV-PD (x-axis)		PSOUMZV-PD (y-axis)	
	A_1	A_1	A_1	$t_2(s)$	$t_3(s)$	$t_2(s)$	$t_3(s)$
Values	1	-1	1	0.2584	0.5988	0.1197	0.6000

4. IMPLEMENTATION AND RESULTS

Simulation tests were conducted on a quadrotor with a suspended payload to confirm the effectiveness of the proposed approach for regulating the system's position and attitude as well as reducing the swing of the payload. The proposed and comparative control algorithms were designed using the MATLAB/ Simulink. The payload mass and cable length were set as 80 g and 1 m respectively. Table 3 presents the system parameters of the quadrotor with a suspended payload. The quadrotor initial position and the desired position are set as $r_o = [0,\ 0,\ 0\ ]^{\mathrm{T}}$ and $r = [0.5,\ 0.5,\ 1.5]^{\mathrm{T}}$ respectively. For performance comparison, the UMZV-PD was implemented as shown in Figure 2. For comparative technique, the UMZV parameters are calculated by using a linearized model [19]. The system's damping ratio was assumed as zero, whereas linearized frequency of the single pendulum dynamic can be calculated as

$$\omega = \sqrt{\frac{g}{l}} \tag{24}$$

The Proportional-Derivative (PD) controllers are utilized for the control of the quadrotor altitude and position for both proposed and comparative methods. Table 3 tabulates the position and altitude controller parameters for the control of quadrotor system.

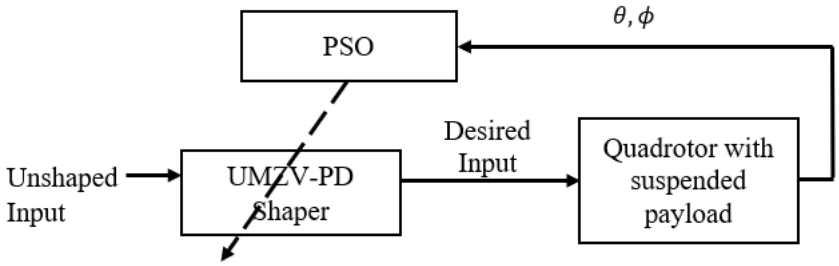

Figure 1. A block diagram of UMZV-PD shaper optimized by PSO.

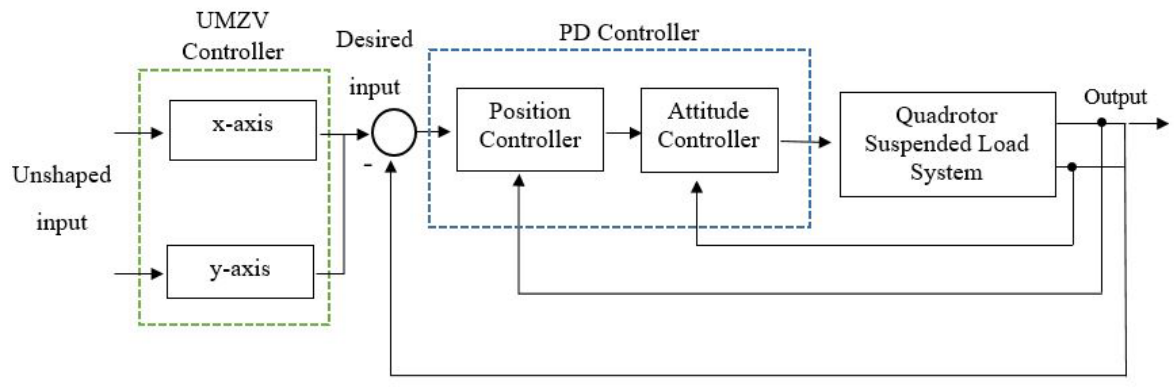

Figure 2. The control structure for comparative method.

Table 4 shows the shapers' parameters for comparative method. A mean square error (MSE) was used as a performance indicator of the overall payload swing response. Hence, a low MSE value is desirable that indicates a minimum overall payload swing. Additionally, residual swing performance was measured between 2 and 10 seconds; a lower payload swing value corresponds to a stronger suppression of residual swing.

The input-shaped signals of the PSO-based UMZV and the linearized model-based UMZV are displayed in Figure 3. It was noted that the proposed and comparative methods recorded 0.6 secs and 0.7 secs of the shaped duration respectively in the x-direction. In y-direction, the proposed and comparative methods obtained 0.62 secs and 0.7 secs of the shaper duration respectively. Hence, the proposed method achieved a faster shaper duration as compared to the comparative method for both the x and y directions.

Figures 4-6 show the quadrotor position, attitude and payload swing responses for the proposed and comparative techniques. Table 5 tabulates the mean square error of the quadrotor position and the attitude responses for both techniques. It was shown that the MSE of quadrotor positions in all direction recorded almost similar results for both proposed and comparative methods indicating the capability of PD controller to achieve the desired quadrotor positions. Analyzing the attitude response with the MSE value, the proposed method recorded improvements of 56.79 %, 31.42 % and 59.98 % for yaw, roll and pitch responses as compared to the comparative method.

Table 3. Position and attitude controller parameters.

Types of controllers/ Parameters	Position Controller		Attitude Controller	
	K_p	K_d	K_p	K_d
Roll	1	2.5	1	0.5
Pitch	1	2	1	0.4
Yaw	-	-	0.5	0.2
Z- Axis	-	-	10	12

Table 4. Shaper's parameters for the comparative method.

Shaper parameters	Amplitude			Time locations (s)			
				UMZV-PD (x-axis)		UMZV-PD (y-axis)	
	A_1	A_1	A_1	$t_2(s)$	$t_{3x}(s)$	$t_2(s)$	$t_3(s)$
UMZV-PD	1	-1	1	0.3343	0.6687	0.3343	0.6687

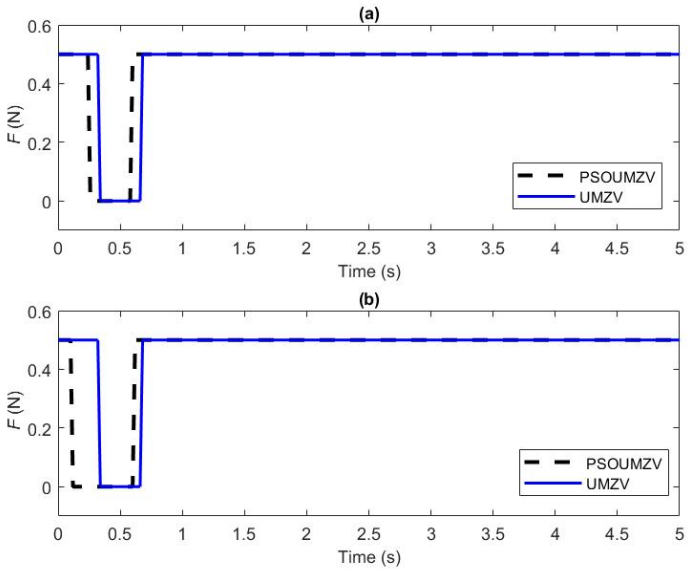

Figure 3. The shaped input responses. (a) x-direction (b) y-direction

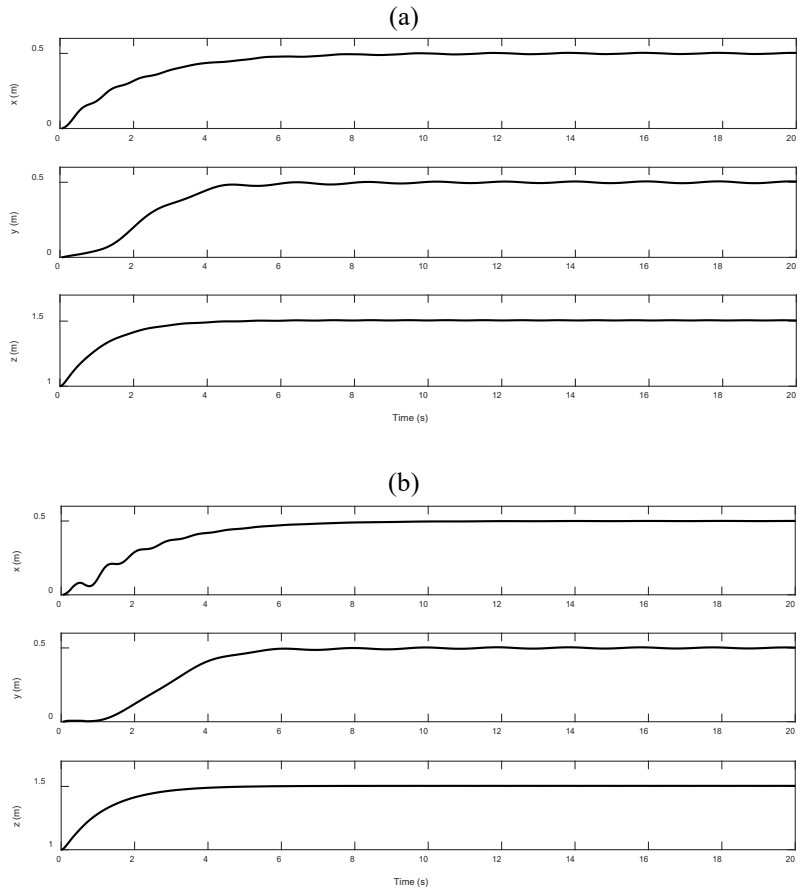

Figure 4. Quadrotor position responses. (a) PSOUMZV-PD (b)UMZV-PD.

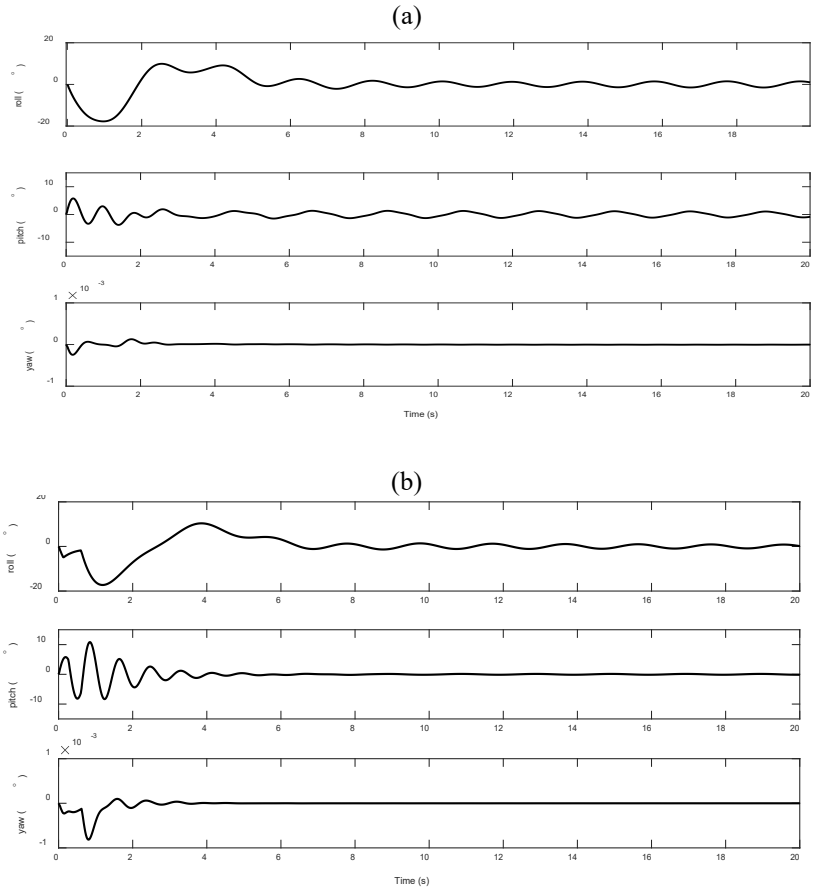

Figure 5. Quadrotor attitude responses (a) PSOUMZV-PD (b)UMZV-PD.

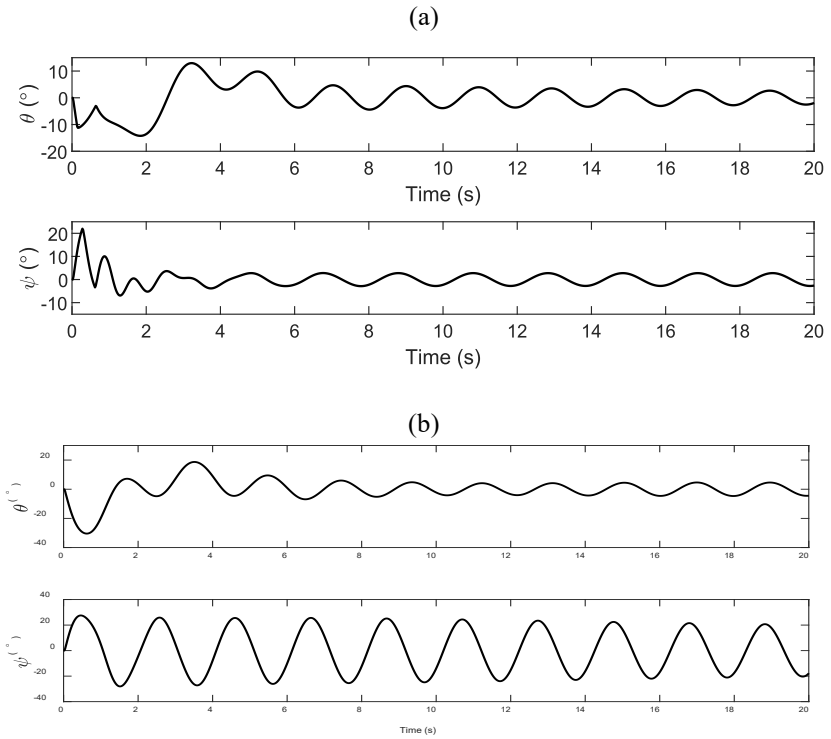

Figure 6. Payload swing responses for the quadrotor system (a) PSOUMZV-PD (b) UMZV-PD.

Table 5. MSE performances for the PSOUMZV-PD and UMZV-PD controllers.

Type of Controller / Characteristics	MSE	
	PSOUMZ-PD	UMZV-PD
Position (x)	0.2164	0.2157
Position (y)	0.2122	0.2125
Position (z)	2.1818	2.19
Yaw	$2.1813e^{-12}$	$5.049e^{-12}$
Roll	0.0048	0.007
Pitch	0.00076584	0.0023

Table 6. Performance index of payload swing responses.

Type of controller	MSE		RS	
	θ	φ	θ	φ
PSOUMZV-PD	0.0067	0.0028	0.0108	0.0014
UMZV-PD	0.0193	0.1390	0.0213	0.1804

Table 6 further demonstrates the superior performance of the suggested controller, which saw improvements in θ and φ of 97.98% and 65.28 percent, respectively, as compared to the comparison approaches for the entire swing. terms of RS, improvements of 99.22 % and 49.29 % for θ and φ were recorded by the proposed method as compared to the comparative method. Noticeably, although a similar controller was used for controlling the quadrotor attitude, the proposed method exhibits better performances of roll, pitch and yaw responses due to a good control of the payload swing responses achieves by the PSO-based UMZV. Besides, this indicates the proficiency of the PSO algorithm optimizing the UMZV parameters based on the non-linear system.

5. CONCLUSION

An improved UMZV shaper approach was presented for efficient payload swing reduction of a quadrotor system carrying a hanging payload. To find the ideal UMZV parameters for shaper design, the PSO method was employed. MATLAB simulations showed that the proposed shaper with PSO able to reduce the payload swing more effectively than the shaper designed using a linear model. Furthermore, the proposed control achieved superior attitude and position performance compared to the conventional method. This indicates the proposed controller is shown to be effective to control the overall system under the coupling between the quadrotor and the payload swing.

ACKNOWLEDGEMENT AND FUNDING

We would like to acknowledge Ministry of Higher Education, Malaysia for Fundamental of Research Grant Scheme, FRGS (FRGS/1/2020/TK0/USIM/02/2) and Faculty of Engineering and Built Environment, USIM for the funding and support.

DECLARATION OF CONFLICTING INTERESTS

The authors declare no potential conflicts of interest with respect to the research and publication of this article.

REFERENCES

[1] A. Farras, A. Santoso and Y. E. Nugraha, Fault-tolerant control for multi-quadcopter with suspended payload under wind disturbance*, Journal on Advanced Research in Electrical Engineering*, 8(2), 2024, 60-66.
[2] J. Estevez, G. Garate, J. M. Lopez-Guede and M. Larrea, Review of aerial transportation of suspended-cable payloads with quadrotors, *Drones*, 8(2), 2024, 35.
[3] H. M. Omar, R. Akram, S. M. S. Mukras and A. A. Mahvouz, Recent advances and challenges in controlling quadrotors with suspended loads, *Alexandria Engineering Journal*, 63, 2023, 253-270.
[4] Y. Fang, X. Liang, N. Sun and H. Lin, Nonlinear hierarchical control for unmanned quadrotor transportation systems*, IEEE Transactions on Industrial Electronics*, 65, 2018, 3395-3405.
[5] H. Ergezer and K. Leblebicioğlu, Control structure design with constraints for a slung load quadrotor system, *Measurement and Control*, 57, 2024, 16-29.
[6] S. Sadr, S. A. A. Moosavian and P. Zarafshan, Dynamics modeling and control of a quadrotor with swing load, *Journal of Robotics*, 2014, 2014, 65897.
[7] P. Zhao, Y. Zhou and R. Zhou, A new trajectory optimizing method using input shaping principles, *Shock and Vibration*, 2018, 4173253.
[8] S. Yang and B. Xian, Energy-based nonlinear adaptive control design for the quadrotor UAV system with a suspended payload, *IEEE Transactions on Industrial Electronics*, 67, 2020, 2054-2064.
[9] J. Cai and B. Xian, Robust hierarchical geometry control for the multiple UAVs aerial transportation system with a suspended payload*, Nonlinear Dynamics*, 112, 2024, 4551-4571.
[10] X. Huo, J. Chen, Q. Liu and X. He, Vibration elimination for quadrotor slung system based on input shaping and double closed-loop control, *12th Asian Control Conference*, Japan, 2019.
[11] N. A. Johnson, *Control of a Folding Quadrotor with a Slung Load Using Input Shaping*, Master Dissertation, Georgia Institute of Technology, Atlanta, USA, 2017.
[12] J. B. Ubbink and J. A. A. Engelbrecht, Sequence-constrained trajectory planning and execution for a quadrotor UAV with suspended payload, *IFAC-PapersOnLine*, 53, 2020, 9405-9411.
[13] S. Ichikawa and H. Kojima, Oscillation suppression control of a quadrotor-borne payload using input shaping, *Proceedings of Conference of Kanto Branch*, 2018, GS0613.
[14] Adams, J. Potter and W. Singhose, Modeling and input shaping control of a micro coaxial radio-controlled helicopter carrying a suspended load, *International Conference on Control, Automation and Systems*, Jeju, Korea, 2012, 645-650.
[15] R. Mar, A. Goyal, V. Nguyen, T. Yang and W. Singhose, Combined input shaping and feedback control for double-pendulum systems, *Mechanical Systems Signal Processing*, 85, 2017, 267-277.
[16] S. Baklouti, E. Courteille, P. Lemoine and S. Caro, Input shaping for feed-forward control of cable-driven parallel robots, *Journal of Dynamic Systems, Measurement and Control*, 143, 2021, 021007.
[17] W. Ha, D. Lee, K. H. Rew and K. S. Kim, An impulse-time perturbation approach for a symmetric extra-insensitive input shaper, *International Journal of Control, Automation, and Systems*, 16, 2018, 1239-1246.
[18] N. Johnson and W. Singhose, Dynamics and modeling of a quadrotor with a suspended payload, *Applied Aerodynamics Conference*, Atlanta, Georgia, 2018.
[19] K. L. Sorensen, K. Hekman and W. E. Singhose, Finite-state input shaping*, IEEE Transactions on Control Systems Technology*, 18, 2010, 664-672.